Protein Engineering, Design & Selection vol. 20 no. 10 pp. 473–480, 2007
Published online October 24, 2007 doi:10.1093/protein/gzm028

Structure-activity correlations in pentachlorobenzene oxidation by engineered cytochrome $P450_{cam}$[1]

Feng Xu[2], Stephen G. Bell[3], Zihe Rao[2,4,5] and Luet-Lok Wong[3,5]

[2]Tsinghua-Nankai-IBP Joint Research Group for Structural Biology, Tsinghua University, Beijing 100084, China, [3]Inorganic Chemistry Laboratory, Department of Chemistry, University of Oxford, South Parks Road, Oxford OX1 3QR, UK and [4]National Laboratory of Biomacromolecules, Institute of Biophysics, Chinese Academy of Sciences, Beijing 100101, China

[5]To whom correspondence should be addressed. E-mail: raozh@xtal.tsinghua.edu.cn (Z.R.); E-mail: luet.wong@chem.ox.ac.uk (L.-L.W.)

[1]The coordinates for the structure of the F87W/Y96F/L244A/V247L mutant complexed with pentachlorobenzene have been deposited in the Protein Data Bank (access code 2GQX).

We had reported engineering of the heme monooxygenase cytochrome $P450_{cam}$ from *Pseudomonas putida* with the F87W/Y96F/L244A/V247L mutations for the oxidation of pentachlorobenzene (PeCB), a recalcitrant environmental contaminant, to pentachlorophenol. In order to provide further insights into P450 structure, function and substrate recognition, we have determined the crystal structure of this 4-mutant without a substrate and its complex with PeCB. PeCB is bound face-on to the heme, with a weak Fe—Cl interaction. One PeCB chlorine is located in the cavity generated by the L244A mutation, in striking illustration of the role of this mutation in promoting PeCB binding. The structures also show that the $P450_{cam}$ oxygen-binding groove between G248 and T252 is flexible and can tolerate significant deviations from their conformations in the wild type without loss of enzyme activity. Analysis of the PeCB binding interactions led to introduction of the T101A mutation to enable the substrate to reorient during the catalytic cycle for more efficient oxidation. The resultant 5-mutant F87W/Y96F/T101A/L244A/V247L is 3-fold more active for PeCB oxidation than the 4-mutant. Polychlorinated benzene binding by the mutants and the partitioning between substrate oxidation and non-productive (uncoupling) side reactions are correlated with the structural data.

Keywords: biodegradation/cytochrome P450/mutagenesis/polychlorinated aromatics/protein engineering

Introduction

Polychlorinated aromatic compounds are environmental pollutants that pose significant hazards due to their lipid solubility, high toxicity and potential carcinogenicity (Fetzner and Lingens, 1994; Robinson and Lenn, 1994; Carpenter, 1998). Their recalcitrance to biodegradation and hence persistence in the environment generally increases with the number of chlorine substituents but also varies with the position of these substituents. For example, the heavily chlorinated compounds pentachlorobenzene (PeCB) and hexachlorobenzene (HCB) are highly resistant to biodegradation, but so is the less substituted congener 1,3,5-trichlorobenzene (TCB). On the other hand, the polychlorinated phenols, which are also pollutants, are more reactive and readily degraded by a wide range of microorganisms (Radehaus and Schmidt, 1992; Orser and Lange, 1994; Leung *et al.*, 1997; Lee *et al.*, 1998; Solyanikova and Golovleva, 1999). We proposed that genetic augmentation of chlorophenol-degrading microorganisms with enzymes that oxidize chlorinated benzenes to the phenols should lead to systems capable of biodegrading the recalcitrant benzene contaminants (Chen *et al.*, 2002).

The cytochrome P450 (CYP) superfamily of heme monooxygenases is ubiquitous in all kingdoms of life. The main activity of P450 enzymes is the catalytic oxidation of C—H bonds in endogenous and exogenous organic molecules (Ortiz de Montellano, 1995; Guengerich, 2001). Substrate oxidation requires two electrons, commonly derived from NAD(P)H, and two protons that are utilized by the heme prosthetic group to activate oxygen to form water and a highly reactive ferryl (Compound I) species that oxidizes the bound substrate (Scheme I). This activity is crucial to biological functions such as biosynthesis of steroids, prostaglandins, hormones and secondary metabolites, as well as oxidative detoxification and degradation of xenobiotics.

The monooxygenase activity of P450 enzymes is potentially of interest in synthesis and other biotechnological applications such as bioremediation and biosensing. The substrate specificity of P450 enzymes is controlled by binding interactions within the active site, while product selectivity depends primarily on the location and accessibility of C—H bonds and functional groups that are close to the oxygen of the ferryl intermediate. P450 enzymes have been shown to be highly amenable to engineering by directed evolution and active site redesign for the oxidation of non-natural substrates (Urlacher and Schmid, 2004, 2006).

We reported the active site redesign of cytochrome $P450_{cam}$ (CYP101A1) from *Pseudomonas putida* (Mueller *et al.*, 1995; Gunsalus and Wagner, 1978) to oxidize polychlorinated benzenes to the phenol derivatives (Jones *et al.*, 2000, 2001). Orders of magnitude increases in activity over the wild type enzyme have been observed with amino acid substitutions at two or three residues (F87, Y96, V247), but the activity decreases with the number of chlorine substituents. The increasing chemical inertness of benzenes with the number of halogen substituents is one factor, but poor substrate binding to the mutant enzyme and incorrect positioning relative to the oxy-ferryl intermediate will also lower the activity. The crystal structure of the F87W/Y96F/V247L mutant (3-mutant) with TCB bound within the active site led to the proposal that binding of PeCB close to the heme, and hence its faster oxidation, could be promoted by introducing the L244A mutation to generate space to accommodate the extra chlorines in PeCB (Chen *et al.*, 2002). Indeed the F87W/Y96F/L244A/V247L mutant (4-mutant) was found to oxidize PeCB to pentachlorophenol (PCP) 45-times faster than the 3-mutant, and HCB was also oxidized to PCP. A catalytically functional gene cassette containing the 4-mutant

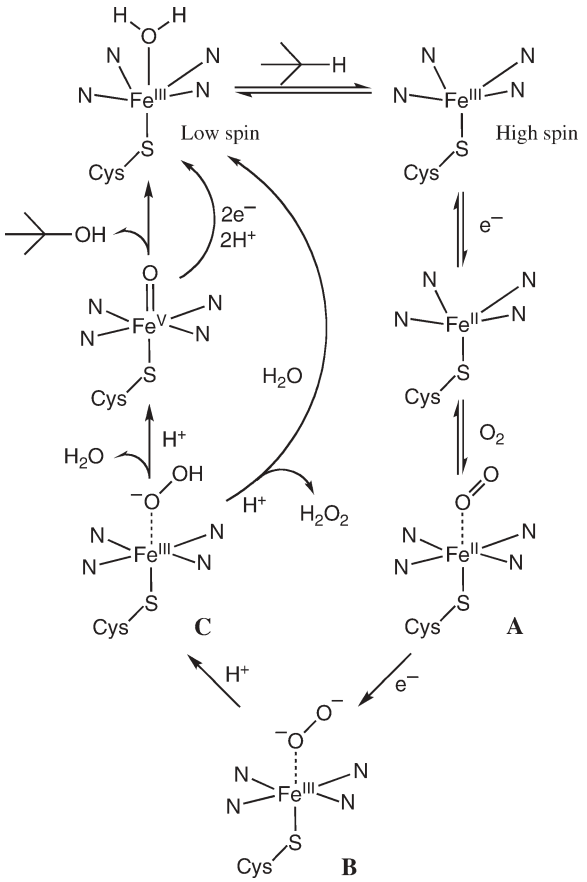

Scheme 1. The general catalytic cycle of P450 enzymes. The overall charge of the heme complex is omitted for clarity. The two electrons required for oxygen activation are delivered stepwise to the heme. Species **A** is the ferrous-oxy, **B** the ferric-peroxy, and **C** the ferric-hydroperoxy form. The dotted lines are used to indicate that the oxygen-derived species (neutral dioxygen in **A**, peroxide O_2^{2-} in **B** and hydroperoxide HO_2^- in **C**) is bound to the iron centre and not the nature of the bonding interaction. The two main pathways of diverting the cycle from product formation: dissociation of hydrogen peroxide and reduction of the ferryl intermediate to the Fe^{III}—OH_2 form (oxidase activity), are also shown.

and the electron transfer proteins has been introduced into a PCP-degrading *Sphingomonas* strain and, as we had proposed, the genetically augmented organism degraded HCB via oxidation to PCP (Yan *et al.*, 2006). There is an continuing interest in microorganisms that can degrade or grow on environmental contaminants such as polyhalogenated aromatic compounds, not only the benzene derivatives but also the biphenyls (Wittich and Wolff, 2007). Oxidation of polychlorinated dioxins to products with greatly reduced toxicity by mutants of $P450_{BM3}$ from *Bacillus megaterium* has been reported (Sulistyaningdyah *et al.*, 2004).

In order to characterize the interaction of non-natural substrates with engineered P450 enzymes, we have determined the crystal structure of the substrate-free form and PeCB complex of the 4-mutant. The structural data are correlated with results from studies on the binding and oxidation of TCB and PeCB by $P450_{cam}$ mutants.

Materials and methods

General

Enzymes for molecular biology were from New England Biolabs, UK. Buffer components were from Anachem, UK. General reagents were from Sigma/Aldrich or Merck, UK. NADH was from Roche Diagnostics, UK. 2-Naphthol, TCB, 2,4,6-trichlorophenol (2,4,6-TCP), PeCB and PCP were from Sigma/Aldrich. UV/Vis spectra and enzymatic assays were recorded at $30 \pm 0.5^{\circ}C$ on a Varian CARY50 spectrophotometer. Gas chromatography (GC) analyses were carried out on a ThermoFisher Trace instrument equipped with an autosampler and a flame-ionization detector (FID) using a 7-m DB-1 fused silica capillary column with helium as the carrier gas.

Enzymes and molecular biology

General DNA and microbiological experiments were carried out by standard methods (Sambrook *et al.*, 1989). Both the 3- and 4-mutant had been described previously (Bell *et al.*, 2001b). The new F87W/Y96F/T101A/L244A/V247L mutant was generated by site-directed mutagenesis using the 4-mutant gene as template. PCR mutagenesis was carried out using the QuikChange kit from Stratagene. The oligonucleotide 5′-tttgacttcattcccgcctcgatggatccgccc-3′ (target codon underlined), together with its reverse complement (MWG Biotech, Germany), were used to generate the T101A mutation. After the PCR mutagenesis step, the amplified product was digested with *Dpn* I to cleave the template DNA. The digested DNA was transformed into *Escherichia coli* XL1-Blue and the bacteria plated on LB agar containing 34 μg/mL chloramphenicol to select for the intact pCHC plasmid harboring the mutant cam*C* gene (Westlake *et al.*, 1999; Bell *et al.*, 2001a). Mutants were identified and then fully sequenced by automated DNA sequencing on an ABI 377XL Prism DNA sequencer by the DNA sequencing facility at the Department of Biochemistry, University of Oxford.

Wild type and mutants of $P450_{cam}$, and the physiological electron transfer co-factor proteins putidaredoxin and putidaredoxin reductase, were expressed in *E.coli* and purified by published methods (Peterson *et al.*, 1990; Yasukochi *et al.*, 1994; Westlake *et al.*, 1999). The purified proteins were stored at $-30^{\circ}C$ in 50 mM Tris, pH 7.4 containing 50% v/v glycerol. Glycerol was removed immediately before all experiments by gel filtration on a 5-mL PD-10 column (GE Healthcare, UK) by eluting with 50 mM Tris, pH 7.4. The concentration of $P450_{cam}$ mutants was determined by the CO-difference spectrum using $\varepsilon_{450} = 91\ mM^{-1}\ cm^{-1}$ (Omura and Sato, 1964), while $\varepsilon_{454} = 10\ mM^{-1}\ cm^{-1}$ was used for putidaredoxin reductase and $\varepsilon_{455} = 10.4\ mM^{-1}\ cm^{-1}$ for putidaredoxin (Gunsalus and Wagner, 1978). The presence or otherwise of the inactive P420 form was assayed for all $P450_{cam}$ mutants at the beginning and end of each set of experiments. None of the enzymes showed any significant tendency of P420 formation either on storage or during experiments where stock solutions were kept on ice.

Crystallization of $P450_{cam}$ and substrate soaking experiments

Crystals of the $P450_{cam}$ 4-mutant were obtained at 291 K by the hanging drop vapor diffusion method reported previously (Chen *et al.*, 2002; Bell *et al.*, 2003), but with minor modifications. Immediately prior to crystallization experiments, the protein was further purified by size exclusion chromatography on a Superdex 75 (GE Healthcare, UK) column (16 mm i.d. × 80 cm), eluting with 50 mM phosphate buffer, pH 7.4, 10 mM β-mercaptoethanol, at a flow rate of 0.8 mL $(min)^{-1}$.

The protein was then buffer exchanged into 100 mM cacodylate, pH 7.2, 200 mM KCl and concentrated to 23 mg(mL)$^{-1}$ by ultrafiltration. A 1.5 μL aliquot of the protein solution was mixed with 1.5 μL of 25% PEG8000 in buffer B (100 mM cacodylate, pH 7.2, 200 mM sodium acetate) and 0.3 μL of 100 mM spermidine in water as additive. The drops were suspended over 200 μL of 25% PEG8000 in buffer B. Diffraction quality crystals appeared within 24 h. The PeCB substrate was soaked into crystals of the substrate-free form of the mutant. The concentration, solvent and soaking time were varied. Crystals were transferred using a fiber loop and soaked in 100 mM MES buffer, pH 7.0, 100 mM sodium acetate, 100 mM KCl, 20% PEG8000 and typically 50 μM PeCB (added as a 10 mM stock solution in DMSO) for 3 days.

Data collection and structure refinement

Immediately prior to data collection, crystals were soaked in a cryoprotecting solution consisting of 100 mM MES buffer (pH 7.0), 100 mM KCl, 100 mM sodium acetate, 20% glycerol and 20% PEG8000, and flash frozen at 100 K in a stream of cold nitrogen gas. X-ray diffraction data were collected at 100 K on a MAR345 or Rigaku R-AXIS IV^{++} image plate using Cu K$_\alpha$ radiation ($\lambda = 1.5418$ Å) from an in-house Rigaku rotating anode X-ray generator operating at 48 kV and 98 mA (RU2000) or 40 kV and 20 mA (MicroMax-007). Data were indexed and scaled by HKL2000 (Otwinowski and Minor, 1997). Model refinement was by CNS and Coot (Brunger *et al.*, 1998; Emsley and Cowtan, 2004).

Crystals of the 4-mutant soaked in a PeCB solution belonged to the $P2_1$ space group, with unit cell dimensions $a = 67.0$ Å, $b = 62.0$ Å, $c = 95.0$ Å, $\alpha = 90^\circ$, $\beta = 89.6^\circ$, $\gamma = 90^\circ$. A total of 245 673 reflections were measured, with R_{merge} of 7.0% for 44 465 unique reflections and 99.9% completeness (50–2.1 Å). Data were collected to 100% completeness in the highest resolution shell. The structure was solved by molecular replacement, based on the crystal structure of wild type P450$_{cam}$ (protein databank code: 2CPP) but with the camphor removed. The difference Fourier map in molecule A in the unit cell showed disc-shaped electron density above the heme that was modeled with a PeCB molecule. The density above the heme in molecule B was modeled with five water molecules. The final refinement parameters were $R_{work} = 19.3\%$ and $R_{free} = 23.6\%$. The relevant statistics are summarized in Table I.

Table I. X-ray data collection, refinement and common structural parameters

	F87W/Y96F/L244A/V247L PeCB complex
Unit cell	$a = 67.0$, $b = 62.0$, $c = 95.0$ Å $\alpha = 90^\circ$, $\beta = 89.6^\circ$, $\gamma = 90^\circ$
Space group	$P2_1$
Number of molecules in asymmetric unit	2
Refinement	26.1–2.1 Å
Unique reflections	44 465
Completeness (highest resolution shell)	99.9% (100%)
Redundancy (highest resolution shell)	5.4 (5.3)
$(I)/[\sigma(I)]$ (highest resolution shell)	13.8 (3.2)
R^a_{merge}	7.0%
Matthews coefficient	2.2
Solvent content	43.5%
R^b_{work}	19.3%
R^b_{free}	23.6%
Residues not modeled	A1–A9, B1–B9
rmsd from restraint values	Bond lengths: 0.006 Å, bond angles: 1.312°
rmsd between C$_\alpha$ backbone of molecules	WT versus A: 0.40 Å; WT versus B: 0.44 Å; A versus B: 0.31 Å
Fe–S (Cys 357) distance (WT: 2.20 Å)	A: 2.24 Å; B: 2.24 Å
Fe–porphyrin plane distance (WT: 0.37 Å)	A: 0.35 Å; B: 0.35 Å
Ramachandran analysis:Most favored (additionally allowed)	87.6% (12.4%)

[a] $R_{merge} = \Sigma|(I) - I|/\Sigma(I)$ over all reflections.
[b] $R_{work} = \Sigma|F_o - F_c|/F_o$ for all reflections, R_{free} was calculated from 8% reflections withheld at random.

Substrate binding assays

Substrate binding was examined at 30°C by the high spin heme content in the presence of an excess of substrate and the substrate binding constant. The substrate-free form of a P450$_{cam}$ enzyme, with a Soret maximum at 418 nm, was prepared by gel filtration through a PD-10 column and diluted to ~5 μM. Substrate binding was detected by a shift of the Soret maximum from 418 nm to 392 nm for the high spin heme upon addition of aliquots of 10 mM stock solutions of TCB and PeCB in DMSO. Further aliquots were added until there was no further change in the spectrum. The high spin heme content was estimated qualitatively to within ~5% by comparing the observed spectrum with a series of mixed high spin/low spin spectra of P450$_{cam}$ calculated by summation of appropriate fractions of the spectra of the substrate-free (>95% low spin) and camphor-bound (>95% high spin) forms of wild type P450$_{cam}$.

Substrate binding constants were determined from the difference spectrum in the range 300–500 nm. The substrate-free form of the P450$_{cam}$ mutant was diluted to 5 μM in a final volume of 1.5 mL containing 50 mM Tris, pH 7.4, 200 mM KCl and 1% v/v DMSO. Stock solutions of TCB and PeCB at 2 mM, 5 mM and 10 mM in DMSO were prepared. The substrate-free spectrum was used as the baseline and the difference spectrum was recorded after successive addition of 1 μL aliquots of substrate solution. A total of 10 μL of substrate solution was added, typically 6 × 1 μL of the 2 mM solution, 2 × 1 μL of 5 mM and 2 × 1 μL of 10 mM. For TCB binding by the F87W/Y96F/T101A/L244A/V247L mutant, which showed a larger dissociation constant, 6 × 1 μL of 5 mM and 4 × 1 μL of 10 mM stock solutions were used. The total volume increase was <1% and the final DMSO concentration was <2% v/v. Control experiments showed that the spectrum of the substrate-free forms were not affected by 2% v/v DMSO. The difference spectra showed a peak at 389 nm and a trough at 420 nm. The peak-to-trough absorbance difference was fitted against the substrate concentration to a hyperbolic function for substrate binding using the Origin7.0 program (Origin Labs).

NADH turnover rate and metabolite determinations

Incubation mixtures (1.5 mL) contained 50 mM Tris, pH 7.4, 1% v/v DMSO, 200 mM KCl, 1 μM P450$_{cam}$, 10 μM putidaredoxin and 1 μM putidaredoxin reductase. The mixtures were oxygenated and then equilibrated at 30°C for 2 min. TCB or PeCB was added as a 10 mM stock in DMSO to a

nominal final concentration of 100 μM. NADH was added to ~160 μM ($A_{340} = 1.00$) and the absorbance at 340 nm monitored. The steady-state rate of NADH turnover was calculated using $\varepsilon_{340} = 6.22\ mM^{-1}\ cm^{-1}$ and given in units of nmol-NADH consumed per nmol-P450 per min.

After all the NADH had been consumed in an incubation reaction, 2-naphthol was added to the mixture to act as an internal standard. Organics in the mixtures were extracted with 0.5 mL of ethyl acetate and the layers separated by centrifugation at 4000 g, 4°C, for 10 min. The organic layer was removed and stored at −20°C before GC analysis. Both the injector and FID were held at 250°C. The column temperature was held at 60°C for 1 min and then increased at 15°C/min to 150°C and held at 150°C for 3 min. The retention times were: 2-naphthol 2.04 min, 2,4,6-TCP 3.41 min, and PCP 6.30 min. The concentration of the 2,4,6-TCP or PCP product was determined by calibrating the FID response. Mixtures containing different concentrations of product and all the components of a normal incubation, except NADH and substrate, were extracted and analyzed as for normal incubations. The plot of the ratio of the product peak area to the 2-naphthol internal standard against the phenol product concentration gave a calibration plot from which the absolute concentration of phenols produced by enzymatic turnover could be determined. The coupling efficiency was the percentage of NADH consumed that lead to product formation.

The concentration of hydrogen peroxide formed by uncoupling during NADH oxidation was determined by the horseradish peroxidase/phenol/4-aminoantipyrine assay. The total assay volume was 800 μL and contained 200 μL of 50 mM Tris, pH 7.4, 400 μL of a TCB or PeCB reaction mixture upon completion of the reaction, 100 μL of 100 mM phenol and 100 μL of 10 mM 4-AP (both in 50 mM Tris pH 7.4). The absorbance at 510 nm (λ_{max} of the quinoneimine coupling product, $\varepsilon_{510} = 6580\ M^{-1}cm^{-1}$) was set to zero, 1 μL of a 20 mg mL^{-1} solution of HRP in water was then added, and the absorbance recorded. The concentration of hydrogen peroxide in a substrate oxidation mixture was calculated from a calibration plot using known concentrations of hydrogen peroxide added to a standard incubation mixture but with NADH omitted. Further control reactions were carried out in which a known concentration of hydrogen peroxide was added to a substrate oxidation incubation mixture which was left to stand for 2 min and then assayed by the method above. The results showed that peroxide concentrations down to 1 μM could be detected.

Results and discussion

Structure of the F87W/Y96F/L244A/V247L (4-mutant) with and without bound PeCB

The structure of the 4-mutant with PeCB bound was determined to examine the structural effect of the mutations, and in particular the role of the L244A mutation in the 45-fold increase in the PeCB oxidation activity over the F87W/Y96F/V247L (3-mutant). Crystals of the 4-mutant were obtained after screening crystallization conditions based on those used for crystallizing the 3-mutant (Chen *et al.*, 2002). Co-crystallization of the protein with the PeCB substrate did not produce diffraction quality crystals. Crystals of the substrate-free form were therefore soaked in buffers containing different concentrations of PeCB and various organic solvents. The best crystals were obtained with DMSO as the co-solvent.

The structure of the PeCB complex has been solved at 2.1 Å resolution by molecular replacement methods. Of the two molecules in the $P2_1$ unit cell, the Fourier difference map for molecule A clearly shows disk shaped electron density above the heme, indicating that a planar PeCB molecule is bound within the active site. The density above the heme in molecule B shows five peaks which are modeled as water molecules. Both protein molecules retain the structural features of the wild type enzyme. Data collection and refinement statistics are summarized in Table I. Since the unit cell conveniently contains the substrate-free and PeCB-bound forms of the enzyme, the effect of the mutations on the structure of the enzyme *per se*, independent of alterations resulting from PeCB binding, are presented first, followed by the PeCB-bound form in order to highlight any differences.

Molecule B in the unit cell is the substrate-free form. The observed electron density and fits for some active site residues and the water molecules are shown in Fig. 1a. The W87 indole NH adopts the 'up' orientation, with a hydrogen bond

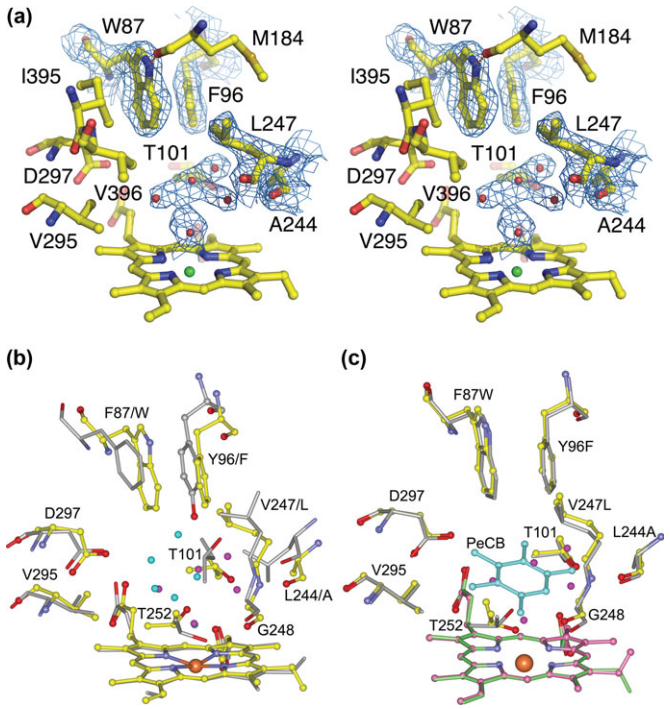

Fig. 1. (**a**) Stereo view of the active site structure of the substrate-free (native) form of the F87W/Y96F/L244A/V247L mutant in molecule B of $P2_1$ space group crystals showing the electron density ($2F_o-F_c$ contoured at 1σ) and fit for the W87 side chain and the hydrogen bond between the indole NH and the carbonyl of M184. There are five ordered water molecules that extend in a branched chain from the heme iron to contact the side chains of T101 and A244. The figure was generated with the program PyMOL. (**b**) Overlay of the structure of the native form of the F87W/Y96F/L244A/V247L mutant (carbon atoms in yellow; active site waters in red) with the wild type (carbon atoms in grey; waters in cyan) showing the location of two water molecules in the cavity generated by the L244A mutation and the altered conformations of A244 and in particular of T252 which breaks the hydrogen bond to the G248 backbone carbonyl. (**c**) Overlay of the native form (carbon atoms in grey) and PeCB complex (carbon atoms in yellow) of the mutant showing the change in the T252 side chain conformation and restoration of the hydrogen bond to G248. Figure (b) and (c) were generated with the program ViewerPro.

to the M184 carbonyl (N—O distance: 2.91 Å) while the benzene ring points downwards at the heme. The density above the heme is well defined and modeled with five water molecules in a branched chain arrangement extending from a heme-bound water (Fe—O 2.56 Å). The substrate-free structures of the 4-mutant and the wild type are overlaid in Fig. 1b. It is clear that two new water molecules are bound in the space generated by the L244A mutation. One of these forms hydrogen bonds with the A244 carbonyl (O—O 2.75 Å) and the other water which is in turn stabilized by a hydrogen bond to the T101 side chain OH (O—O 2.89 Å). Both these waters are hydrogen bonded with the fourth active site water (O—O 2.50 and 2.71 Å). The fifth water is located over pyrrole A. Another significant difference is the side chain conformation of T252. The hydrogen bond in the wild type between the T252 side chain OH and carbonyl oxygen of G248 is broken in the mutant (O—O 3.52 Å) because of a rotation of the T252 side chain, resulting in the G248/T252 oxygen-binding groove being opened up in the mutant and potentially interfering with oxygen binding and activation.

Molecule A in the unit cell is the PeCB complex. The substrate electron density above the heme is modeled with a PeCB molecule that is almost symmetrically disposed between pyrroles A and D and the *meso* carbon CH_A (Fig. 2a). There are extensive van der Waals contacts between PeCB and the porphyrin. The angle between the planes of the two aromatic systems is 20°, compared to 28° for the TCB complex with the 3-mutant. A chlorine atom of PeCB is coordinated to the heme iron but with a long Fe—Cl distance (3.32 Å), and this iron-bound chlorine also forms a hydrogen bond with the T252 side chain OH (Cl—O 3.01 Å). One chlorine is accommodated in the space created by the L244A mutation. This chlorine contacts the A244 C_α (3.90 Å) and methyl (3.99 Å), and forms a hydrogen bond with the T101 OH (Cl—O 3.45 Å). The unique CH in PeCB contacts G248. There are also numerous van der Waals and polar contacts between the PeCB chlorines and other active site residues, including W87, F96, L247, G248, T252, V295, D297 and V396.

The structure of the PeCB complex is compared to the substrate-free form of the mutant (Fig. 1c), and the wild type enzyme complexed with its natural substrate, camphor (Fig. 2b). Like the camphor complex of the wild type, all the active site waters are displaced when PeCB binds to the 4-mutant. As observed for the substrate-free form, the W87 indole NH in the PeCB complex is oriented upwards to form a hydrogen bond with the M184 carbonyl (N—O 3.02 Å) while the benzene ring points downwards and contacts the PeCB chlorines. The W87, F96 and A244 side chains remain in their positions while G248 moves closer to the heme iron. The T252 side chain rotates to avoid steric hindrance with the Fe—Cl, which brings the side chain OH group to form a hydrogen bond with the G248 carbonyl oxygen. Although the conformations of G248 and T252 remain different from their counterparts in the wild type (Fig. 2b), this hydrogen bond (O—O 2.71 Å compared to 2.60 Å in the wild type) restores the 248/252 oxygen-binding groove.

In contrast to the PeCB complex of the 4-mutant, the TCB binding orientations in the previously reported structure of the TCB complex of the 3-mutant have the W87 side chain NH in the 'down' orientation (Chen *et al.*, 2002). Hydrogen bonding between the indole NH and a TCB chlorine is an important factor. Compared to the parallel binding orientation of TCB in the 3-mutant (Fig. 2c), PeCB in the 4-mutant is rotated by ~30° about the carbon closest to the heme iron such that a chlorine occupies the space generated by the L244A mutation and no PeCB chlorine is sufficiently close to the W87 side chain for hydrogen bonding. As a result, there is no driving force to break the W87–M184 hydrogen bond. The 'indole NH up' orientation of the W87 side chain also maximizes van der Waals contact between the indole benzene ring and the PeCB chlorines.

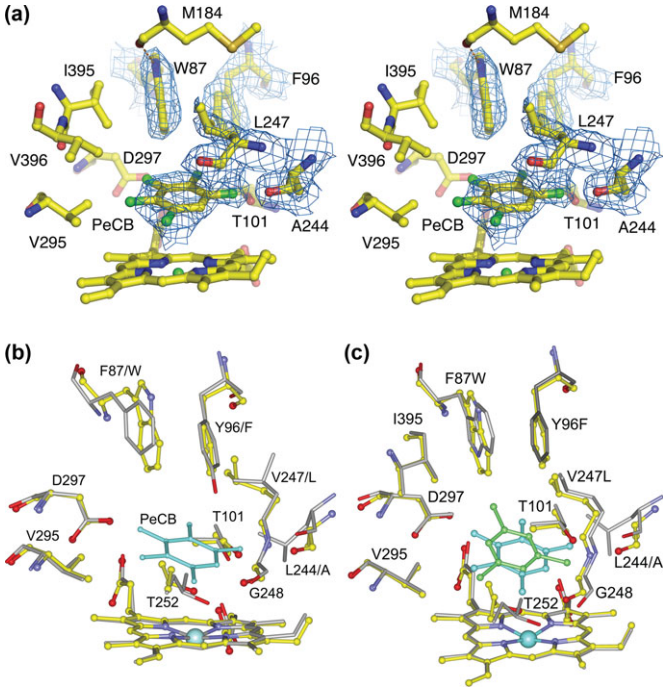

Fig. 2. (**a**) Stereo view of the active site structure of the PeCB complex of the F87W/Y96F/L244A/V247L mutant in molecule A showing the electron density ($2F_o-F_c$ contoured at 1σ) and fit for the PeCB substrate. One PeCB chlorine is coordinated to the heme iron while another chlorine is located in the cavity generated by the L244A mutation. The W87 indole NH points upward and form a hydrogen bond with the carbonyl of M184. The figure was generated with the program PyMOL. (**b**) Overlay of the active site structure of the PeCB complex of the mutant (carbons in yellow) with the camphor complex of wild type $P450_{cam}$ (carbons in grey) showing movements of A244, G248 and T252. Camphor has been omitted for clarity. (**c**) Overlay of the structure of the PeCB complex of the F87W/Y96F/L244A/V247L mutant (carbons in yellow) with the TCB complex of the F87W/Y96F/V247L mutant (carbons in grey) showing the rotation of PeCB relative to TCB about the carbon closest to the heme iron and the altered conformations of A244, G248 and T252 in the PeCB complex. Figure (b) and (c) were generated with the program ViewerPro.

Structure-activity correlations

The crystal structures provide a useful framework for comparing the data for TCB and PeCB binding and oxidation by the 3- and 4-mutant (Table II). As reported previously, the 3-mutant does not have sufficient space to accommodate PeCB while TCB can bind in the productive, near-parallel orientation with a C—H bond poised over the heme iron, giving ~65% high-spin heme content, good NADH turnover activity and coupling (product yield) (Chen *et al.*, 2002). The crystal structure of the 4-mutant shows that the overall effect of the L244A mutation is to create space to promote binding of PeCB in the productive near-parallel orientation, leading

Table II. Catalytic parameters for the oxidation of 1,3,5-TCB and PeCB by wild type and mutants of P450cam (CYP101A1)

P450cam enzyme	1,3,5-TCB					PeCB				
	% HS	K_d (μM)	NADH rate (Product rate)	Coupling	H_2O_2	% HS	K_d (μM)	NADH rate (Product rate)	Coupling	H_2O_2
Wild type[a]	<5%	–	6.40 ± 1.2 (0.07 ± 0.02)	1.1 ± 0.3%	–	<5%	–	3.0 ± 1.5 (*n.d.*)	*n.d.*	–
F87W/Y96F/V247L[a]	70%	2.07 ± 0.17[b]	308.0 ± 21.5 (175.0 ± 6.1)	56.8 ± 3.2%	2.7 ± 1.4%[b]	<5%	–	91.0 ± 2.3 (1.8 ± 0.18)	1.9 ± 0.2%	2.7 ± 1.3%[b]
F87W/Y96F/L244A/V247L[b]	<5%	–	286.2 ± 17.2 (54.5 ± 2.2)	19.1 ± 0.54%	2.6 ± 1.6%	55%	2.03 ± 0.15	311.0 ± 11.2 (82.5 ± 2.4)	24.0 ± 1.8%	1.5 ± 0.9%
F87W/Y96F/T101A/L244A/V247L[b]	15%	19.5 ± 1.82	365.7 ± 7.5 (88.5 ± 3.5)	24.2 ± 0.85%	2.9 ± 1.3%	65%	1.71 ± 0.14	481.2 ± 31.2 (214.4 ± 12.7)	45.9 ± 1.5%	1.4 ± 0.7%

% HS (to ±5%) is the high spin heme content in the presence of excess substrate. The other data are given as mean ± S.D. for at least three experiments. The NADH turnover rate and the product formation rate (2,4,6-trichlorophenol, 2,4,6-TCP, for 1,3,5-TCB; pentachlorophenol, PCP, for PeCB) are given in nmol (nmol P450cam)$^{-1}$ min^{-1}. Coupling is the percentage of NADH consumed that led to product formation. H_2O_2 is the percentage of NADH consumed that was diverted to form peroxide via uncoupling. *n.d.*: no product observed; –: no reliable value could be determined.
[a]Data from (Chen *et al.*, 2002).
[b]This work.

to increased PeCB oxidation activity (Chen *et al.*, 2002). Since C—Cl bonds are highly resistant to oxidation, PeCB is preferentially oxidized to PCP. The PeCB binding constant of the 4-mutant ($K_d = 2.03 \pm 0.15$ μM) has been determined in the present work and found to be identical to that for TCB binding by the 3-mutant ($K_d = 2.07 \pm 0.17$ μM).

The Fe—Cl interaction in the 4-mutant PeCB complex might be expected to lead to a low-spin heme, in contradiction to the ∼55% high-spin heme content observed at 30°C in solution (Chen *et al.*, 2002). It is possible that the heme coordination in solution is different from that in the crystal, e.g. the Fe—Cl interaction may be broken and the heme becomes 5-coordinate or a water molecule enters the active site and binds to the heme iron. However, these changes may not be necessary since the neutral chlorine is a poor donor ligand to iron because it is a substituent on an electron-withdrawing benzene ring containing four other chlorines. Moreover, the structure shows that the Fe—Cl also accepts a hydrogen bond from the T252 side chain OH, which will further reduce its donor strength. These factors are reflected in the long Fe—Cl distance of 3.32 Å; by comparison the Fe—S distance to the proximal cysteine thiolate is 2.24 Å. Whatever the nature of the heme-sixth ligand interaction, it is clear that the activation energy for the rate-limiting first electron transfer step, and hence the steady-state NADH turnover rates, for TCB oxidation by the 3-mutant and PeCB oxidation by the 4-mutant (Table II), are virtually identical.

Despite identical NADH turnover rates, the PeCB oxidation product formation rate for the 4-mutant is lower than that for TCB oxidation by the 3-mutant because the product yield based on NADH consumed (coupling efficiency) for PeCB oxidation (24.0%) is lower than that for TCB (56.8%). There are three uncoupling side reactions that compete with product formation in the P450 catalytic cycle (Scheme 1) and hence reduce the product yield (Mueller *et al.*, 1995). Superoxide can dissociate from the ferrous-oxy form and disproportionate to hydrogen peroxide. Peroxide can dissociate from the ferric-hydroperoxy species, especially if delivery of the second proton required for O—O bond cleavage is disrupted, or if water enters the active site and protonates the heme-bound oxygen atom. The third pathway is reduction of the ferryl species by two electrons back to the ferric form (Scheme 1). This pathway leads to the overall 4-electron reduction of oxygen to water, i.e. oxidase activity, and is expected to occur if the substrate is bound too far away from the ferryl or if the group closest to the heme iron is inert to oxidation. Substrate oxidation by the ferryl is slowed down and the normally slower process of electron transfer reduction of the ferryl by the co-factor protein can compete with product formation.

In the present work, we have analyzed the reaction products and found that virtually no hydrogen peroxide (<3%) is formed in PeCB or TCB oxidation by wild type $P450_{cam}$ and the mutants (Table II), indicating that oxidase activity is the dominant uncoupling mechanism in these reactions. These observations have two significant implications. Firstly, the L244A mutation causes movement of G248 and T252 in the 4-mutant. These two residues, via hydrogen bonding, play crucial roles in oxygen binding and activation to form the ferryl intermediate (Schlichting *et al.*, 2000). Incorrect positioning of the side chains may weaken oxygen binding

and slow down O—O bond cleavage sufficiently to lead to hydrogen peroxide formation. The low peroxide concentrations therefore indicate that the $P450_{cam}$ enzyme can tolerate significant perturbations to the oxygen-binding groove without losing catalytic activity.

Secondly, the greater extent of oxidase uncoupling for PeCB oxidation by the 4-mutant is most likely due to the higher probability of a chemically inert C—Cl bond being close to the ferryl species. The PeCB complex of the 4-mutant has a chlorine closest to the heme iron while TCB is bound in the 3-mutant with a C—H bond over the heme iron. We therefore hypothesized that, if the PeCB chlorines can move away from the heme iron, the molecule can rotate to bring the C—H and C=C bonds closer to the ferryl oxygen and increase the likelihood of substrate oxidation and hence the coupling yield. These movements may occur with the T101A mutation which allows the substrate to slide towards the 101 side chain while preserving other van der Waals contacts, e.g. with the porphyrin, for substrate binding.

Effect of the T101A mutation

As shown in Table II, introduction of the T101A mutation does not significantly affect PeCB binding (K_d 1.71 $\pm$ 0.14 μM), but increases the high spin heme content (~65%), the rate of NADH turnover (481 min^{-1}), and nearly doubles the coupling yield (45.9%). The increased high-spin heme content and faster NADH rate are consistent with a weaker Fe—Cl interaction or loss of such an interaction altogether, as space is created to enable the PeCB to move away from the heme iron. Uncoupling via hydrogen peroxide remains low (<3%). Therefore, oxidase activity is still the dominant uncoupling pathway but its extent is much reduced in the 5-mutant F87W/Y96F/T101A/L244A/V247L because the inert PeCB C—Cl bonds can move away from the oxygen of the ferryl. The PCP product formation rate of the 5-mutant (214 min^{-1}) is nearly 3 times as fast as that for the 4-mutant, and indeed faster than TCB oxidation by the 3-mutant. The cumulative effect of adding the L244A and T101A mutations to the 3-mutant on PeCB oxidation is remarkable in view of the low solubility and chemical inertness of PeCB.

The effect of adding the T101A mutation on TCB oxidation is mixed. There are modest increases in the high spin heme content, NADH turnover activity and coupling over the 4-mutant, but TCB binding is ~10-fold weaker than PeCB binding. The T101A mutation has made the active site in the 5-mutant too large for tight TCB binding. It slightly increased the coupling yield over the 4-mutant but the 3-mutant remains the most active for TCB oxidation.

Summary and conclusions

The crystal structure of the PeCB complex of mutant F87W/Y96F/L244A/V247L (4-mutant) of cytochrome $P450_{cam}$ shows the polychlorinated benzene to be bound with the ring almost parallel to the heme. Chlorine occupies the space generated by the L244A mutation and there is a Fe—Cl bond. The L244A mutation disrupts the G248/T252 oxygen-binding groove in the substrate-free form and to a lesser extent in the PeCB complex but oxygen binding and activation are not sufficiently affected to lead to uncoupling to form hydrogen peroxide. These observations emphasize the flexibility and adaptability of the P450 fold. Addition of the T101A mutation to the 4-mutant significantly reduces oxidase uncoupling, resulting in greatly increased PeCB oxidation activity and efficiency. The structure determination and functional studies have provided new insights into the binding and oxidation of substituted aromatic compounds by P450 enzymes and how these can be manipulated by protein engineering.

Acknowledgments

The work is supported by grants from Project 863 (Grant number 2005BA711A05-02) of the Ministry of Science and Technology of China, the National Science Foundation of China (Grant number 30221003) (to Z.R.), and by the Biotechnology and Biological Sciences Research Council, UK (Grant number E12666) and the Higher Education Funding Council for England (to L.-L.W.).

References

Bell,S.G., Chen,X., Sowden,R.J., Xu,F., Williams,J.N., Wong,L.L. and Rao,Z. (2003) *J. Am. Chem. Soc.*, **125**, 705–714.
Bell,S.G., Harford-Cross,C.F. and Wong,L.L. (2001) *Protein Eng.*, **14**, 797–802.
Bell,S.G., Sowden,R.J. and Wong,L.-L. (2001) *Chem. Commun.*, 635–636.
Brunger,A.T., *et al*. (1998) *Acta Crystallogr. D Biol. Crystallogr.*, **54**, 905–921.
Carpenter,D.O. (1998) *Int. J. Occup. Med. Environ. Health*, **11**, 291–303.
Chen,X., Christopher,A., Jones,J.P., Bell,S.G., Guo,Q., Xu,F., Rao,Z. and Wong,L.L. (2002) *J. Biol. Chem.*, **277**, 37519–37526.
Emsley,P. and Cowtan,K. (2004) *Acta Crystallogr. D Biol. Crystallogr.*, **60**, 2126–2132.
Fetzner,S. and Lingens,F. (1994) *Microbiol. Rev.*, **58**, 641–685.
Guengerich,F.P. (2001) *Chem. Res. Toxicol.*, **14**, 611–650.
Gunsalus,I.C. and Wagner,G.C. (1978) *Methods Enzymol.*, **52**, 166–188.
Jones,J.P., O'Hare,E.J. and Wong,L.L. (2000) *Chem. Commun.*, 247–248.
Jones,J.P., O'Hare,E.J. and Wong,L.L. (2001) *Eur. J. Biochem.*, **268**, 1460–1467.
Lee,S.G., Yoon,B.D., Park,Y.H. and Oh,H.M. (1998) *J. Appl. Microbiol.*, **85**, 1–8.
Leung,K.T., Cassidy,M.B., Shaw,K.W., Lee,H., Trevors,J.T., Lohnmeier Vogel,E.M. and Vogel,H.J. (1997) *World J. Microbiol. Biotechnol.*, **13**, 305–313.
Mueller,E.J., Loida,P.J. and Sligar,S.G. (1995) In Ortiz de Montellano,P.R. (ed.), *Cytochrome P450: Structure, Mechanism, and Biochemistry* (2nd). Plenum Press, New York, pp. 83–124.
Omura,T. and Sato,R. (1964) *J. Biol. Chem.*, **239**, 2370–2378.
Orser,C.S. and Lange,C.C. (1994) *Biodegradation*, **5**, 277–288.
Ortiz de Montellano,P.R. (1995) *Cytochrome P450: Structure, Mechanism, and Biochemistry*, 2nd edn. Plenum Press, New York.
Otwinowski,Z. and Minor,W. (1997) In Carter,C.W. and Sweet,R.M. (ed), *Methods Enzymol.* Academic Press, pp. 307–326.
Peterson,J.A., Lorence,M.C. and Amarneh,B. (1990) *J. Biol. Chem.*, **265**, 6066–6073.
Radehaus,P.M. and Schmidt,S.K. (1992) *Appl. Environ. Microbiol.*, **58**, 2879–2885.
Robinson,G.K. and Lenn,M.J. (1994) *Biotechnol. Genet. Eng. Rev.*, **12**, 139–188.
Sambrook,J., Fritsch,E.F. and Maniatis,T. (1989) *Molecular Cloning: A Laboratory Manual*, 2nd edn. Cold Spring Harbor Laboratory Press, New York.
Schlichting,I., Berendzen,J., Chu,K., Stock,A.M., Maves,S.A., Benson,D.E., Sweet,R.M., Ringe,D., Petsko,G.A. and Sligar,S.G. (2000) *Science*, **287**, 1615–1622.
Solyanikova,I.P. and Golovleva,L.A. (1999) *Biochemistry (Moscow)*, **64**, 365–372.
Sulistyaningdyah,W.T., Ogawa,J., Li,Q.S., Shinkyo,R., Sakaki,T., Inouye,K., Schmid,R.D. and Shimizu,S. (2004) *Biotechnol. Lett.*, **26**, 1857–1860.
Urlacher,V.B. and Schmid,R.D. (2004) *Methods Enzymol.*, **388**, 208–224.
Urlacher,V.B. and Schmid,R.D. (2006) *Curr. Opin. Chem. Biol.*, **10**, 156–161.
Westlake,A.C., Harford-Cross,C.F., Donovan,J. and Wong,L.L. (1999) *Eur. J. Biochem.*, **265**, 929–935.
Wittich,R.M. and Wolff,P. (2007) *Microbiology*, **153**, 186–195.

Yan,D.Z., Liu,H. and Zhou,N.Y. (2006) *Appl. Environ. Microbiol.*, **72**, 2283–2286.
Yasukochi,T., Okada,O., Hara,T., Sagara,Y., Sekimizu,K. and Horiuchi,T. (1994) *Biochim. Biophys. Acta*, **1204**, 84–90.

Received March 22, 2007; revised May 12, 2007; accepted May 15, 2007

Edited by Frances Arnold